Science Advances

AAAS

advances.sciencemag.org/cgi/content/full/2/11/e1601335/DC1

Supplementary Materials for

Feedforward and feedback frequency-dependent interactions in a large-scale laminar network of the primate cortex

Jorge F. Mejias, John D. Murray, Henry Kennedy, Xiao-Jing Wang

Published 16 November 2016, *Sci. Adv.* **2**, e1601335 (2016)
DOI: 10.1126/sciadv.1601335

This PDF file includes:

- Supplementary Methods
- fig. S1. Microstimulation experiments at the interareal level, for an FB projection that is strong to L2/3E and weak to L5E (more precisely, with a supra/infra ratio of 0.8).
- fig. S2. FLN connectivity matrix, after a logarithmic transformation for visualization purposes, for the 30 areas of the large-scale model.
- fig. S3. SLN connectivity matrix for the 30 areas of the large-scale model.
- fig. S4. Wiring distances, in millimeters, for the 30 areas of the large-scale model.
- fig. S5. Anatomical hierarchy obtained from the data shown in fig. S3.
- fig. S6. Different matrices for the subset of eight areas of interest (V1, V2, V4, DP, 8m, 8l, TEO, and 7A) used in the functional hierarchy study.
- fig. S7. Spectral pairwise-conditioned GC profiles for all the possible pairs of interactions between the eight cortical areas of interest: V1, V2, V4, DP, 8m, 8l, TEO, and 7A, with a background input of $I = 6$ to all areas, plus a strong extra input of $I = 6$ to V1.
- fig. S8. Effect of introducing a distance-dependent relationship on the target of FB projections.

Supplementary Methods

1 General scheme of the model

Here we describe the large-scale model used in the main text and its four different levels of description: (*i*) local populations that describe the activity within a given layer, (*ii*) inter-laminar circuits coupling supragranular and infragranular layers, (*iii*) inter-areal couplings which consider the layer-specific influences between two given cortical areas (such as V1 and V4), and (*iv*) large-scale laminar cortical network, which uses the anatomical connectivity data from (Markov et al., 2011; Markov et al., 2014) to expand the model to a network of 30 cortical areas distributed among occipital, temporal, parietal and frontal lobes.

1.1 Intra-laminar local circuit

We consider two recurrently connected populations, one of excitatory and one of inhibitory neurons, as the typical microcircuit describing the neuronal circuit within a given cortical layer. The dynamics of these populations are described by Wilson-Cowan equations of the form

$$\tau_E \frac{dr_E}{dt} = -r_E + \Phi(I_E^{net} + I_E^{ext}) + \sqrt{\tau_E}\ \xi_E(t) \tag{1}$$

$$\tau_I \frac{dr_I}{dt} = -r_I + \Phi(I_I^{net} + I_I^{ext}) + \sqrt{\tau_I}\ \xi_I(t) \tag{2}$$

where $r_{E,I}$ are the (dimensionless) mean firing rates of the excitatory and inhibitory populations, respectively, $\tau_{E,I}$ are the corresponding time constants, $\xi_{E,I}$ are Gaussian white noise terms of strengths $\sigma_{E,I}$, and $\Phi(x) \equiv x/(1-e^{-x})$ is the transduction function. The network input, $I_{E,I}^{net}$, is the input arriving to the corresponding population (the excitatory and inhibitory one, respectively) from other populations in the network (from the same layer, a different layer, or different areas), and the term $I_{E,I}^{ext}$ is the input from external sources such as sensory stimuli, thalamic input, or cortical areas not explicitly included in the model. Taking into account only local contributions (i.e. assuming an isolated intra-lamninar populations) the network input is given by

$$I_E^{net} = J_{EE}\ r_E + J_{EI}\ r_I \tag{3}$$

$$I_I^{net} = J_{IE}\ r_E + J_{II}\ r_I \tag{4}$$

where $J_{\alpha\beta}$ is the mean synaptic strength from population β to population α. For the circuit in the superficial layer, parameter values are $\tau_E = 6\ ms$, $\tau_I = 15\ ms$, $J_{EE} = 1.5$, $J_{IE} = 3.5$, $J_{EI} = -3.25$, $J_{II} = -2.5$, and $\sigma_{E,I} = 0.3$. For the infragranular circuit, parameters are the same except for $\tau_E = 30\ ms$, $\tau_I = 75\ ms$, and $\sigma_{E,I} = 0.45$. With these parameter values, the circuit displays irregular, noise-driven oscillations in the gamma (supragranular) or alpha (infragranular) rhythms, as shown in Fig. 2a of the main text.

1.2 Inter-laminar interactions

To couple the supragranular and infragranular layers together, we take into account inter-laminar connectivity strength estimated from anatomical (Dantzker and Callaway, 2000; Binzegger et al., 2004; Xu and Callaway, 2009) and phisiological (Thomson et al., 2002) studies, as in (Potjans and Diesmann, 2014). For simplicity, we keep only the strongest connections in each direction between layer 2/3 and layer 5, which are the excitatory projections from layer 2/3 pyramidal neurons to layer 5 pyramidal neurons (with strength $J_{5,2}$), and the ones from layer 5 pyramidal neurons to layer 2/3 interneurons (with strength $J_{2,5}$) as reported in (Dantzker and Callaway, 2000; Xu and Callaway, 2009). Our hypothesis is that these strong projections serve as an estimation of the effective connectivity between both layers, and that a certain set of core features of inter-laminar oscillatory entrainment can be explained in this framework.

Following estimations by (Potjans and Diesmann, 2014) for these projections, we set $J_{5,2} = 1$ and $J_{2,5} = 0.75$. Using a matrix notation for convenience, and considering only intra-laminar and inter-laminar projections, the input arriving to each one of the four populations of a given cortical area is

$$\begin{bmatrix} I_{L2E} \\ I_{L2I} \\ I_{L5E} \\ I_{L5I} \end{bmatrix} = \begin{bmatrix} J_{EE} & J_{EI} & 0 & 0 \\ J_{IE} & J_{II} & J_{2,5} & 0 \\ J_{5,2} & 0 & J_{EE} & J_{EI} \\ 0 & 0 & J_{IE} & J_{II} \end{bmatrix} \times \begin{bmatrix} r_{L2E} \\ r_{L2I} \\ r_{L5E} \\ r_{L5I} \end{bmatrix} \tag{5}$$

where subindexes indicate the specific population and layer. We can rewrite the above expression, for a given area α, as $\mathbf{I}_\alpha = \mathbf{J}_\alpha\ \mathbf{r}_\alpha$.

1.3 Inter-areal interactions

We now define the layer-specific connectivity pattern between two cortical areas (such as V1 and V4, which we will take as an example here). This pattern strongly depends on the positions of the areas relative to each other in the anatomical hierarchy (Felleman and Van Essen, 1991; Markov et al., 2014). For simplicity purposes, we assume a pure feedforward (FF) relationship in the direction V1→V4, and a pure feedback (FB) relationship in the opposite direction (in the large-scale level we will consider more generic cases). According to (Felleman and Van Essen, 1991; Markov et al., 2014), FF projections originate on superficial layers, and they tend to target layer 4, which projects to layer

2/3 afterwards. We therefore assume that the input to populations in area V4, receiving both internal contributions and a pure FF input from V1, is

$$\mathbf{I}_{V4} \equiv \begin{bmatrix} I_{V4L2E} \\ I_{V4L2I} \\ I_{V4L5E} \\ I_{V4L5I} \end{bmatrix} = \mathbf{J}_{V4}\mathbf{r}_{V4} + \begin{bmatrix} J_{FF1} & 0 & 0 & 0 \\ 0 & 0 & 0 & 0 \\ 0 & 0 & 0 & 0 \\ 0 & 0 & 0 & 0 \end{bmatrix} \times \begin{bmatrix} r_{V1L2E} \\ r_{V1L2I} \\ r_{V1L5E} \\ r_{V1L5I} \end{bmatrix} \tag{6}$$

which we can again rewrite as $\mathbf{I}_{V4} = \mathbf{J}_{V4}\mathbf{r}_{V4} + \mathbf{J}_{FF}\ \mathbf{r}_{V1}$.

Feedback projections, on the other hand, stem from infragranular layers (Felleman and Van Essen, 1991; Markov et al., 2014) and tend to target both supragranular and infragranular layers while avoiding layer 4. We assume that FB projections target all four types of populations in V1, with stronger projections arriving at L5E and weaker projections arriving at L2E. The input to V1 would then be

$$\mathbf{I}_{V1} \equiv \begin{bmatrix} I_{V1L2E} \\ I_{V1L2I} \\ I_{V1L5E} \\ I_{V1L5I} \end{bmatrix} = \mathbf{J}_{V1}\mathbf{r}_{V1} + \begin{bmatrix} 0 & 0 & J_{FB1} & 0 \\ 0 & 0 & J_{FB2} & 0 \\ 0 & 0 & J_{FB3} & 0 \\ 0 & 0 & J_{FB4} & 0 \end{bmatrix} \times \begin{bmatrix} r_{V4L2E} \\ r_{V4L2I} \\ r_{V4L5E} \\ r_{V4L5I} \end{bmatrix} \tag{7}$$

which we rewrite as $\mathbf{I}_{V1} = \mathbf{J}_{V1}\mathbf{r}_{V1} + \mathbf{J}_{FB}\ \mathbf{r}_{V4}$. Parameter values for the FF and FB projections are $J_{FF1} = 1$, $J_{FB1} = 0.1$, $J_{FB2} = 0.5$, $J_{FB3} = 0.9$, and $J_{FB4} = 0.5$. Other values for the FB projections, in which the ratio FB1/FB3 is higher, have been also explored (see fig. S1).

1.4 Large-scale network

The inter-areal level is extended to a large-scale cortical network of 30 areas using the anatomical data (Markov et al., 2011; Markova et al., 2013; Markov et al., 2014) and the novel data for LIP. The list of areas and a visual representation of its anatomical projections are shown in fig. S2, S3 and S4, and can be downloaded from core-nets.org. For situations in which data shows subdivisions of a given area (such as in the projection from V2 to LIP, which considers several subdivisions of V2), an average value is considered. The corresponding anatomical hierarchy (computed as in (Chaudhuri et al., 2015)) is shown in fig. S5, and the anatomical properties of a subset of areas of interest is displayed in fig. S6. Anatomically speaking, the relationship between two areas can only rarely be characterized as purely FF or FB (which would correspond to SLN values of one or zero, respectively), but are instead somewhere in the middle (i.e. their SLN value is between both extremes). To reflect this fact, the input received by area i from area j can be generally written as

$$\mathbf{I}_{ij} = \mathrm{SLN}_{ij}\ \mathbf{J}_{FF}\ \mathbf{r}_j + (1 - \mathrm{SLN}_{ij})\ \mathbf{J}_{FB}\ \mathbf{r}_j \tag{8}$$

so that a connection with $\mathrm{SLN}_{ij} = 1$ would be a purely FF projection, and $\mathrm{SLN}_{ij} = 0$ a purely FB connection.

We use the FLN data as a proxy for the strength of inter-areal projections. Since the range of FLN values is very broad (around five orders of magnitude), simply using FLN values as projection strengths would make the majority of

the connections irrelevant for the dynamics of the network. To reproduce, with our rate-based model, the significant inter-areal interactions found in (Bastos et al., 2015), we use a log-linear transformation $w_{ij} = c_1 \mathrm{FLN}_{ij}^{c_2}$, which preserves the connectivity information while compressing the connection values to a range that is more convenient for rate models, and which is similar to previous estimates of the range of effective connectivity in neural circuits (Song et al., 2005). Parameter values used are $c_1 = 1.2$ and $c_2 = 0.3$, but using other parameter values or transformations do not qualitatively change our results.

Merging these two factors together, we obtain the scalar weights $W_{FF}^{ij} \equiv w_{ij}\ \mathrm{SLN}_{ij}$ and $W_{FB}^{ij} \equiv w_{ij}\ (1-\mathrm{SLN}_{ij})$. The input received by neural populations within area i from all other areas at time t is then given by

$$\mathbf{I}_i(t) = \mathbf{J}_i \mathbf{r}_i(t) + \sum_{j \neq i}^{\text{areas}} [W_{FF}^{ij}\ \mathbf{J}_{FF} + W_{FB}^{ij}\ \mathbf{J}_{FB}]\ \mathbf{r}_j(t - \Delta_{ij}) \tag{9}$$

Note that, due to the large distance between areas, inter-areal communication delays can not be ignored (especially when looking at transmission of gamma rhythms). The inter-areal delays Δ_{ij} introduced here were obtained from the wiring distance between anatomical areas as in (Markova et al., 2013), and assuming a signal propagation speed of $\sim 1.5\ m/s$ (Swadlow, 1990; Ferraina et al., 2002; Chaudhuri et al., 2015).

2 Data analysis

2.1 Phase-amplitude coupling

To compute the peak-centered LFP measurement in Fig. 3b in the main text, we band-pass filtered the L5E time series (which presented a spectrum peak at $\sim 9.5\ Hz$ under external stimulation of $I^{ext} = 6$ to L2E and $I^{ext} = 8$ to L5E) between 7 and 12 Hz, and we invert the filtered signal to account for the inverse relationship between the LFP and the mean firing rate. We then divided the filtered time series in segments of duration 4 seconds each, and align these segments with respect to their highest peak (gray lines in the figure). The average of these curves is an alpha-peak-centered estimation of the L5 LFP (blue line in the figure, a time window of five alpha cycles is shown). For the upper panel, we compute the spectrogram of L2E (sliding window of width equal to five gamma cycles, 95% window overlap) and apply the same segmentation process, to display the alpha-phase-locked modulation of gamma power.

2.2 Coherence and Granger causality

We consider that the signal recorded from a given area (as in (van Kerkoerle et al., 2014)) can be approximated by $S(t) = (1-\eta)\ r_{L2E}(t) + \eta\ r_{L5E}(t)$, with the parameter η reflecting the penetration depth of the recording electrode. We use the value $\eta = 0.8$, which reflects the strong impact of apical dendrites of layer 5 pyramidal neurons on the recorded signal, although other values can also be used without drastically changing the results. This is also approximately valid to estimate ECoG measurements, which capture both gamma and alpha rhythms effectively in spite of recording only at the surface.

For the calculation of signal coherence between areas $V1$ and $V4$, we use a temporal sliding window of 4 seconds with 50% sliding overlap over the temporal series $S_{V1}(t)$ and $S_{V4}(t)$. To compute the spectral pairwise conditional Granger causality between the same pair of areas, we use the Multi-Variable Granger Causality Toolbox (Barnett and Seth, 2014) with an optimal AIC model order of up to 120 ms. Spectral Granger causality profiles between eight areas of interest (V1, V2, V4, DP, 8m, 8l, TEO and 7A) are shown in fig. S7.

We follow the definition of (Bastos et al., 2015) for the directed asymmetry index, or DAI, which establishes a frequency-specific directionality of the interactions between to areas. The DAI from area $V1$ to area $V4$, for instance, is defined as the normalized difference between the Granger causality measurements in both directions, or

$$DAI_{V1\rightarrow V4}(f) = \frac{GC_{V1\rightarrow V4}(f) - GC_{V4\rightarrow V1}(f)}{GC_{V1\rightarrow V4}(f) + GC_{V4\rightarrow V1}(f)} \tag{10}$$

We obtain the multi-frequency directed asymmetry index (mDAI) between two areas by averaging their DAI at the gamma and alpha ranges (after changing the sign of the alpha contribution, since it is negatively correlated with SLNs):

$$mDAI_{V1\rightarrow V4} = \frac{DAI_{V1\rightarrow V4}(\gamma) - DAI_{V1\rightarrow V4}(\alpha)}{2} \tag{11}$$

where the DAI for a given frequency range ω is

$$DAI(\omega) = \int_{\omega_{min}}^{\omega_{max}} DAI(f)dt \tag{12}$$

For the purposes of computing mDAI values, we consider $[30,\ 70]$ Hz as the gamma frequency range and $[6,\ 18]$ Hz as the alpha/low beta range.

2.3 Functional hierarchy

To compute the functional hierarchy between the areas considered (V1, V2, V4, DP, 8m, 8l, TEO and 7A), we follow the same procedure as in (Bastos et al., 2015). We first rescale all mDAI values so that they fall within the range $[-5, 5]$. After that, we consider each area in turn as a seed area, and the mDAI values of this seed area relative to all areas are shifted –so that the minimum mDAI value for that seed area is one. By averaging over all seeds we obtain a measurement of the functional hierarchy. We repeat the process and average over five measurements to obtain the functional hierarchy and its corresponding SEM values.

The calculation of the hierarchy requires mutiple computations of spectral pairwise conditioned GC profiles, and the time series fed to the GC toolbox need to have both a high resolution (for gamma oscillations) and long duration (for alpha oscillations). We paralelized the computations using the Matlab Parallelization Toolbox in addition to custom parallelization routines in the NYU high performance computing cluster, to obtain the model results and GC profiles within a reasonable computation time.

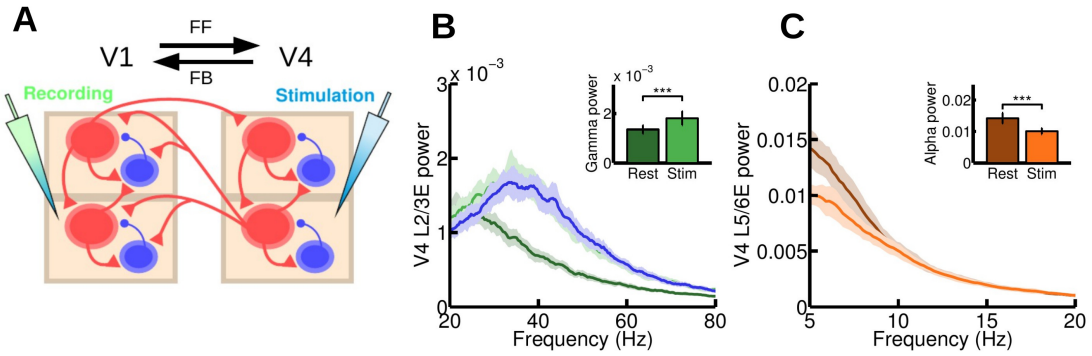

fig. S1. Microstimulation experiments at the inter-areal level, for a FB projection which is strong to L2/3E and weak to L5E (more precisely, with a supra/infra ratio of 0.8). (A) Scheme of the inter-areal projections between two areas, the anatomical hierarchy ascends from left to right. We inject a current of I=15 at all excitatory populations of V4 and recording in V1. A background current of I=1 to all excitatory areas in V1 and V4 is injected, to guarantee a minimum of activity. (B, C) Power spectrum at V1 measured at layer 2/3 (B) and layer 5 (C), for resting and stimulation conditions. Inset show the peak value of the power spectrum for these conditions. A highly significant decrease ($p<0.001$) in alpha power and increase ($p<0.001$) in gamma power were found, suggesting a plausible link between this FB connectivity motif and anatomical pathways associated with top-down attention signals. The blue curve in panel B corresponds to an isolated area receiving the same input as in the stimulation case, but without its rhythmic component (see main text for details).

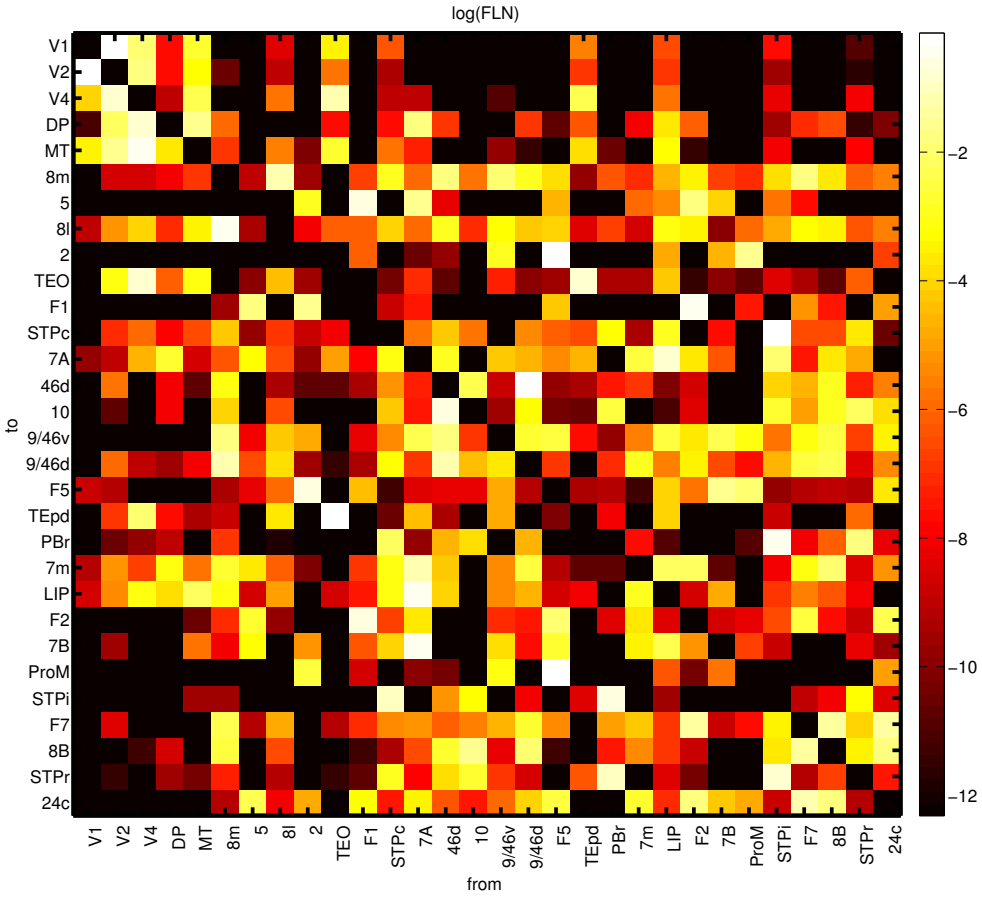

fig. S2. FLN connectivity matrix, after a logarhythmic transformation for visualization purposes, for the 30 areas of the large-scale model. Data is available from core-nets.org.

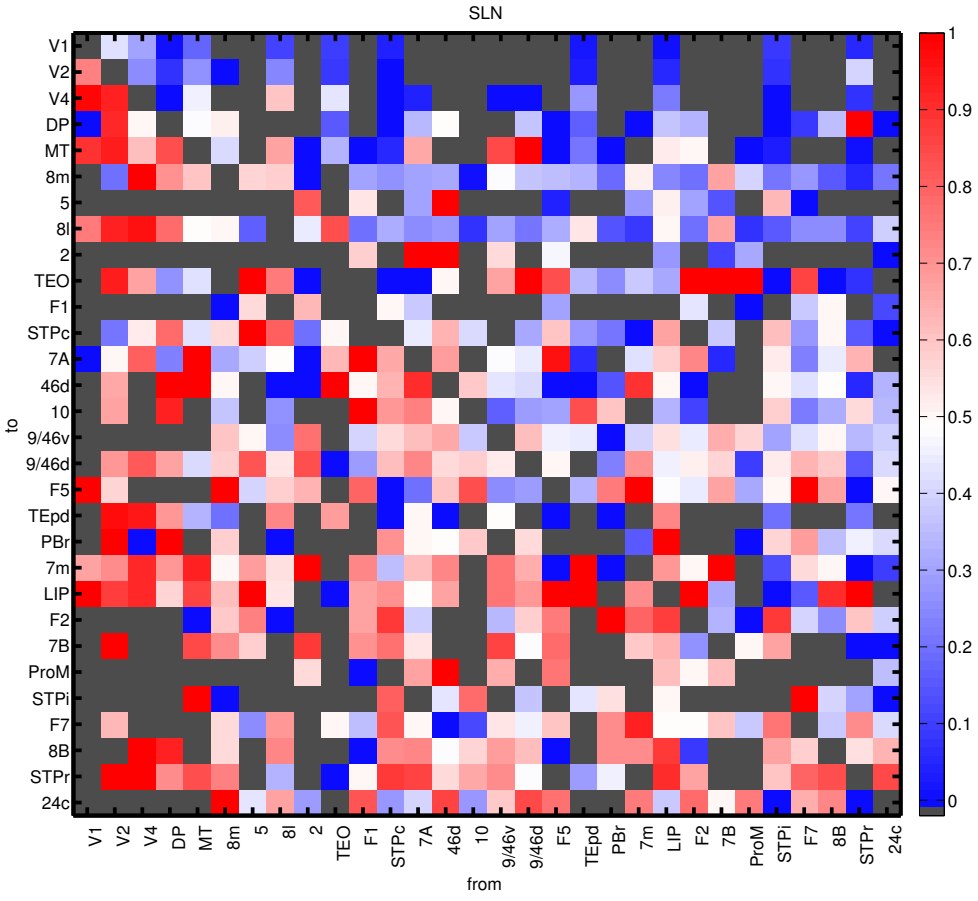

fig. S3. SLN connectivity matrix for the 30 areas of the large-scale model. Grey squares indicate absence of projection. Data is available from core-nets.org.

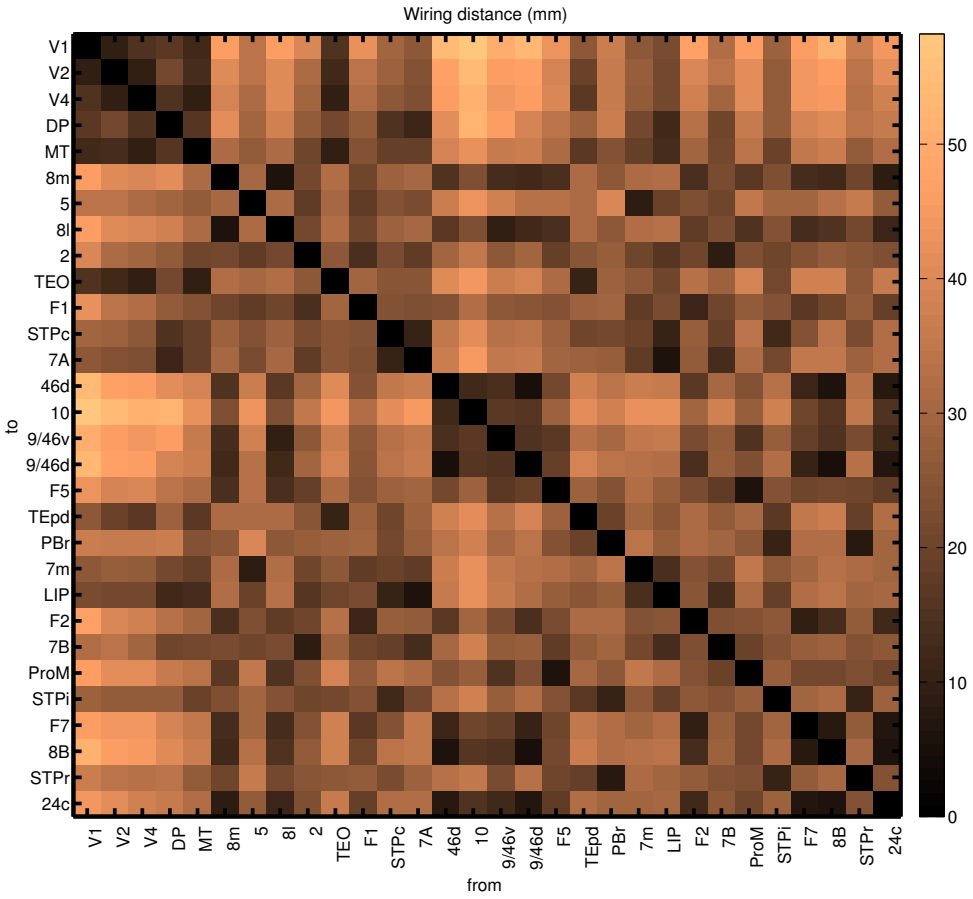

fig. S4. Wiring distances, in mm, for the 30 areas of the large-scale model. Data is available from core-nets.org.

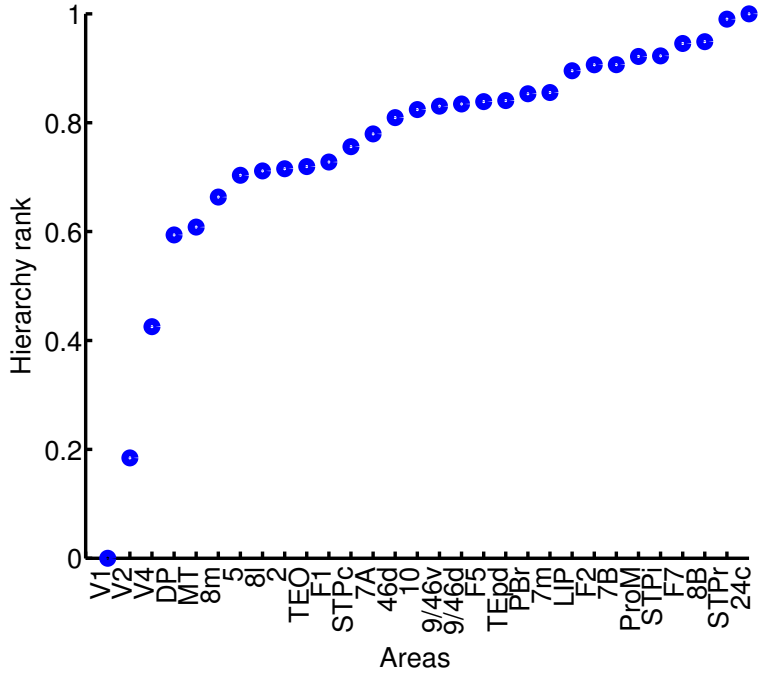

fig. S5. Anatomical hierarchy obtained from the data shown in fig. S3. To accommodate each area within its optimal hierarchical rank (consistently with the SLN values), we have used a generalized linear model as in (Chaudhuri et al., 2015; Markov et al., 2014), but now with the additional area LIP.

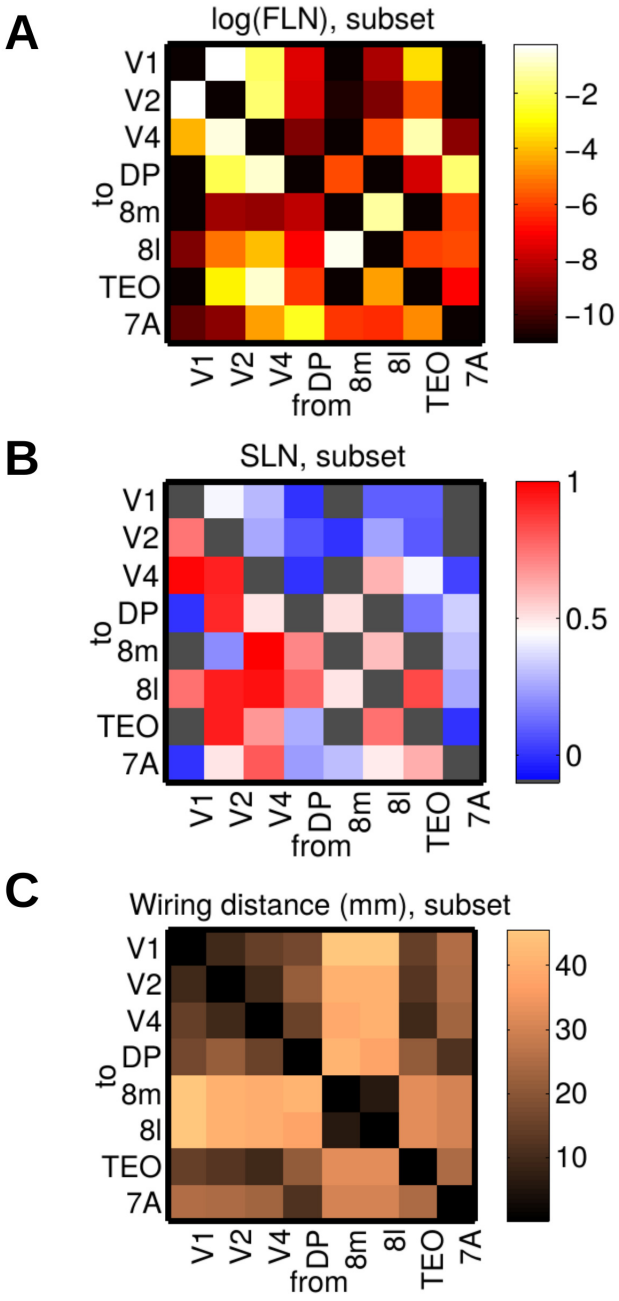

fig. S6. Different matrices for the subset of eight areas of interest (V1, V2, V4, DP, 8m, 8l, TEO, and 7A) used in the functional hierarchy study. Panels correspond to (A) FLN, presented after a logarhythmic transformation, (B) SLN, and (C) wiring distance in mm. For SLNs, grey squares indicate absence of projection.

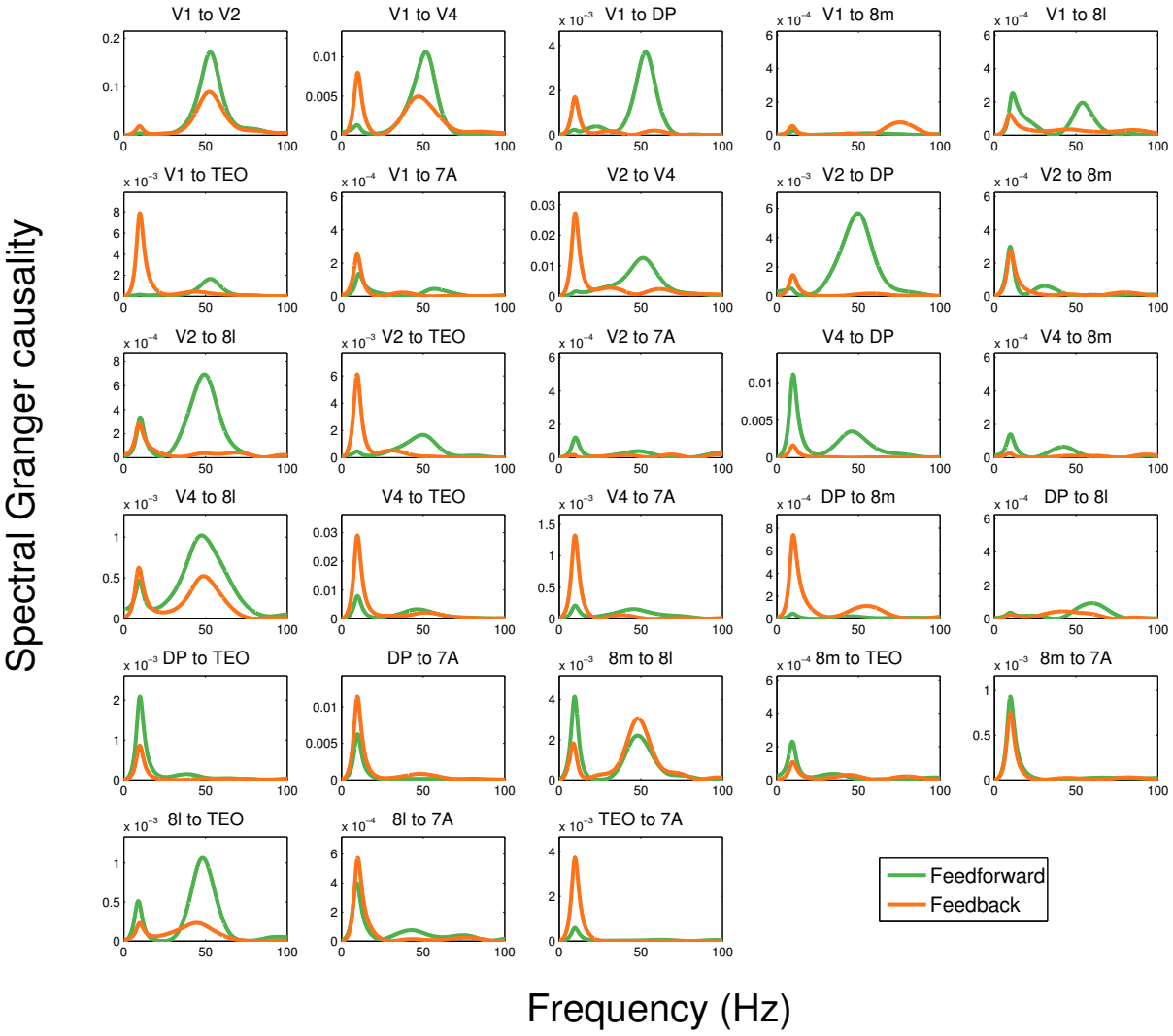

fig. S7. Spectral pair-wise conditioned Granger causality profiles for all the possible pairs of interactions between the eight cortical areas of interest: V1, V2, V4, DP, 8m, 8l, TEO, and 7A, with a background input of I=6 to all areas, plus a strong extra input of I=6 to V1. GC was computed following the same procedure as for Fig. 5 of the main text. A significant gamma/alpha component in the FF/FB direction, respectively, is observed in a consistent manner.

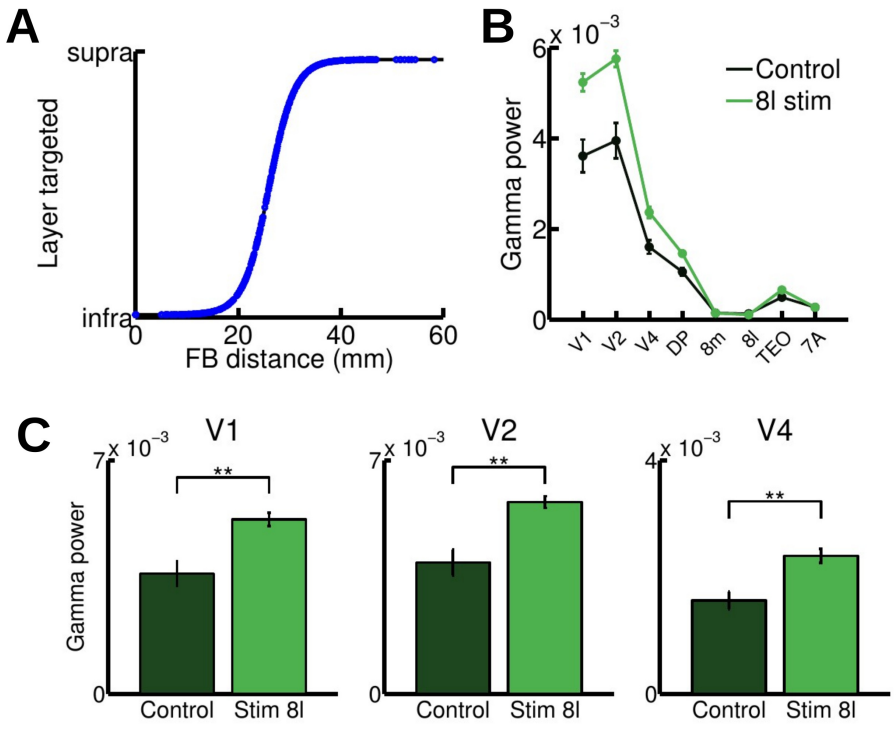

fig. S8. Effect of introducing a distance-dependent relationship on the target of FB projections. (A) Sigmoidal relationship between the FB projection distance and the laminar target (black line) and position of each projection (blue dots). Short-range FB projections will mostly target excitatory neurons in L5/6, while long-range FB projections will target excitatory neurons in L2/3. Other relations, such as a linear dependence, give qualitatively similar results. (B) Simulation of the 30-area large-scale network with this new distance-dependent rule. When L5/6E in area 8l is stimulated (I=8, green line), gamma power for visual areas V1, V2 and V4 is strongly enhanced with respect to the control case (I=0, black line). A slightly stronger inter-areal coupling value (c1=2.4) is used for this stimulation. (C) Differences in the gamma power of the visual areas (control vs FEF-stimulation) in more detail.